Optical properties of Li-based nonlinear crystals for high power mid-IR OPCPA pumped at 1 μm under realistic operational conditions

MAHESH NAMBOODIRI,[1] CHENG LUO,[1] GREGOR INDORF,[2] TORSTEN GOLZ,[2] IVANKA GRGURAŠ,[2] JAN H. BUSS,[2] MICHAEL SCHULZ,[2] ROBERT RIEDEL,[2] MARK J. PRANDOLINI,[2,3,5] AND TIM LAARMANN[1,4,6]

[1]*Deutsches Elektronen-Synchrotron DESY, Notkestraße 85, 22607 Hamburg, Germany*
[2]*Class 5 Photonics GmbH, Notkestraße 85, 22607 Hamburg, Germany*
[3]*Universität Hamburg, Institut für Experimentalphysik, Luruper Chaussee 149, 22761, Hamburg, Germany*
[4]*The Hamburg Centre for Ultrafast Imaging CUI, 22761 Hamburg, Germany*
[5]*mark.prandolini@desy.de*
[6]*tim.laarmann@desy.de*

Abstract: Optical properties of mid-infrared, Li-based nonlinear crystals (NLC) are estimated under realistic experimental conditions for high power lasers using the thermal imaging method. The study focuses on crystals with relatively large apertures for high energy and power applications that are transparent in a broad spectral range (6–16 μm). For this purpose, a high average power Yb:YAG laser amplifier system was used that pumps the crystals and the thermal response of the materials was recorded. An estimate of the linear and nonlinear absorption coefficients of different non-oxide crystals at the 1-μm pump wavelength along with their nonlinear refractive index is provided. To the best of our knowledge, linear and nonlinear absorption coefficients are presented for the first time, including the nonlinear refractive index of AGS, LGSe, LIS, and LISe. These optical material properties are of utmost importance for cutting-edge laser developments close to damage thresholds since they affect the resulting beam quality and conversion efficiencies of novel high power optical parametric amplifiers operating in the long-wavelength mid-infrared spectral range.

1. Introduction

Mid-infrared (mid-IR) optical parametric chirped-pulse amplifier (OPCPA) laser systems operating at central wavelengths beyond 5 μm and delivering ultrashort pulses at high repetition rate and high power levels are of considerable interest for vibrational spectroscopy, label-free microscopy and ultrafast dynamic studies [1]. The dream to efficiently control matter, materials and building blocks of life with light beyond electronic excitations, pushes the development of both the mid-IR laser sources and sophisticated laser pulse shaping capabilities in this spectral range [2]. Due to the exceptional power scalability of 1 μm Yb pump lasers, OPAs operating between 3 and 4 μm have been developed that provide femtosecond laser pulses at MHz-rate on the multiple watt-level [3–8]. These lasers rely on wide-bandgap oxide crystals for parametric frequency down-conversion, which are available commercially with aperture sizes well above 1 cm. Different nonlinear optical materials such as $LiNbO_3$, $KNbO_3$, and $KTiOAsO_4$ (KTA) can be pumped with short (< 1.5 ps) pulse high power lasers with negligible two-photon absorption at 1 μm and high damage threshold [9,10]. Since oxide crystals exhibit strong multiphoton absorption bands in the spectral range above 5 μm, one typically has to build an OPA-DFG (difference frequency generation) cascade to reach the longer-wave mid-IR range. In corresponding laser schemes, the OPA stages uses oxide crystals, and the DFG stage is based on non-oxide

semiconductor crystals, such as $AgGaSe_2$ [11,12], GaSe [2,13–15], $AgGaS_2$ [16,17], $CdSiP_2$ [18] and $ZnGeP_2$ [19–21]. The bandgap of these materials is rather small, i.e. on the order of the 2.4 eV, which matches the two-photon energy of high power commercial Yb pump lasers. It excludes or at least makes it extremely challenging to efficiently pump a parametric frequency down-conversion process in these crystals at 1 μm without damage [22].

The overall pump-to-mid-IR energy conversion efficiency of the OPA/DFG cascades is typically well below 0.5% at a center wavelength of $\approx$ 8 μm. Thus, eliminating the usual difference frequency generation step in producing laser pulses in the limit of long wavelength ($\lambda \geq 5$ μm) holds the promise to increase the conversion efficiency of parametric down-conversion devices significantly. As a prerequisite, novel non-oxide Li-based materials – $LiGaS_2$ (LGS), $LiGaSe_2$ (LGSe), LIS ($LiInS_2$), and $LiInSe_2$ (LISe) – are becoming available that are transparent in a broad spectral range across the mid-IR (6–16 μm) and exhibit sufficiently large damage threshold. Combined with high-average power 1-μm Yb pump laser technology this opens up the door to extend ultrashort high power laser pulses for research, development and industry applications towards the longer-wave mid-IR. Impressive results have been achieved recently by using the LGS crystals, which exhibit a transparency range of 0.32–11.6 μm and have a large bandgap of $\approx$ 4 eV. Ultrashort pulses on the nanojoule-level with a pulse duration close to the Fourier-transform limit at central wavelengths ranging from 7–11 μm have been demonstrated in OPA [23–25], DFG [13], and intra-pulse DFG laser systems [7,26,27]. On the one hand, further scaling up of the pulse energy and average power of the LGS-based mid-IR lasers is constrained in DFG- and OPA-schemes, due to the current limitations in the available crystal aperture size ($\approx 7 \times 7$ mm^2) at larger lengths ($\approx$ 5–7 mm). On the other hand, it has been suggested that in OPCPA systems, up-scaling of the pulse energy beyond 100 μJ and watt-level average power should in principle be straightforward by using longer crystals (several mm) and longer pump pulse width ($\approx$ 10 ps) [1]. Of course, at some point the damage threshold of LGS at peak intensity, on the order of 50 GW/cm^2, comes into play [23]. But even before, when pumped at 1 μm with ultrashort pulses at MHz repetition rate it is crucial to control the resulting thermal loads. Insufficient heat conductivity may result in temperature gradients across the crystal. Spatially inhomogeneous refractive index changes can occur, which lead to varying phase-matching conditions across the crystal, limiting the attainable average power, the spectral bandwidth, the beam quality and compromise the stable and reliable long-term performance. Thus, in order to design robust mid-IR laser architectures detailed information on the optical properties of the converter materials under realistic high power and energy conditions is essential [28]. However, investigations of material properties related to ultrafast laser-induced damage in nonlinear crystals at repetition rates above a few kHz are rare [29].

An easy to implement thermal imaging method gives a good upper limit estimate of the linear and nonlinear absorption coefficients, including the nonlinear refractive index "under operational conditions" [30]. This means that the material parameters are measured using the same laser pump parameters as that which would be used for high energy and power OPCPA-pumping. In this case, a high power laser is irradiating the entire surface area of a large crystal (with aperture 9×9 mm^2). These measurements provide a more realistic absorption and nonlinear coefficients averaging over large crystals with local volume defects, impurities, surface effects and surface defects. Thus, the thermal imaging method provides realistic upper limits compared to methods measuring locally inside a small "perfect" crystals [30]. In comparison, the well-established photothermal common-path interferometry PCI technique [31] yields only linear absorption, very accurately and punctually within the crystal volume using a low power continuous wave laser and thus multi-photon absorption coefficient is not measured with this method. Additionally, the well-known z-scan method, introduced in 1990 by van Stryland and co-workers [32], provides accurately the nonlinear refractive index n_2 within a small volume of the crystal.

We have selected a few of the non-oxide, nonlinear crystals (NLC) for the present study and derive their linear and two-photon absorption coefficients along with the nonlinear refractive index, cf. Table 1 at 1.03 μm, using a commercial Yb:YAG Innoslab from AMPHOS. The laser system provides $\tau = 0.92$ ps (FWHM, fitted with a sech^2 function) pulses at $\lambda_0 = 1030$ nm (spectral bandwidth ≈ 1.1 nm), $M^2 < 1.3$ and a tunable repetition rate from 200 kHz up to 1 MHz. Similar average power levels can be obtained at both repetition rates with maximum output power $P = 200 \pm 2$ W.

Table 1. Optical properties of mid-IR non-oxide, Li-based nonlinear crystals

nonlinear crystal	Bandgap [36] [eV]	d_{eff} [37] [pm/V]	α [cm^{-1}]	β [cm/GW]	n_2 cm^2/W
			derived constants for 1030 nm wavelength		
AgGaS$_2$ (AGS)	2.70	15.9	< 0.005	-	$< 140.6 \times 10^{-15}$
LiGaS$_2$ (LGS)	4.15	5.60	< 0.002	$< 3.2 \times 10^{-4}$	$< 6.4 \times 10^{-15}$
LiGaSe$_2$ (LGSe)	3.34	9.27	< 0.002	$< 2.0 \times 10^{-3}$	$< 27.4 \times 10^{-15}$
LiInS$_2$ (LIS)	3.57	6.90	< 0.001	$< 2.6 \times 10^{-4}$	$< 9.4 \times 10^{-15}$
LiInSe$_2$ (LISe)	2.86	9.48	< 0.01	$< 1.6 \times 10^{-3}$	$< 16.2 \times 10^{-15}$

2. Experimental set-up and samples

The experimental setup is depicted in Fig. 1. All NLCs were placed on two ceramic stands, where only the bottom corners were in contact with the crystals and fixed from the top using a nylon tip screw; such that all surfaces were exposed to ambient air flow, and thus, thermal conduction to the holder is kept to a minimum. The "free-standing" NLCs were irradiated by the 1 μm laser beam under real application like conditions. The experiments were conducted at 1 MHz and 200 kHz repetition rate, and by using a half-wave plate and polarizer, the average power at each repetition rate can be changed. The laser beam sizes were similar in both cases (1/e^2 radius $\omega = 2.1$ mm), which was adjusted to fill the complete crystal aperture (9 × 9 mm^2) in order to obtain a homogeneous heat distribution across the crystal. The experiments were performed on LGS (type II-XY plane, θ = 90°; φ = 37.5°), LGSe (type II-XY plane, θ = 90°; φ = 33.5°), LIS (type II-XY plane, θ = 90°; φ = 31.5°), LISe (type II-XY plane, θ = 90°; φ = 33.0°) and AGS (type II-XY plane, θ = 90°; φ = 39.5°). The 2 mm thick crystals were commercially bought from the vendor Ascut Ltd.&Co.KG [28]. The crystals were uncoated on both sides and the cut angle is selected for 10 μm idler wavelength when pumped at 1.03 μm. All measurements were performed with pump laser in "e" polarization. The reflected and transmitted pump laser powers were measured to estimate the power inside the crystal and Fresnel reflections at both front and back surfaces, resulting in a reduction of about 13.4% of the total power. The beam profile of the transmitted beam was monitored (Basler Aca 1300gm) by reflecting a small part of it using a wedge. The thermal images of the crystals under investigation were recorded in thermal equilibrium using an IR camera (FLUKE Ti25, spectral range 7.5–14 μm). A typical example of the heat distribution of a pumped crystal is presented in Fig. 1 (bottom, left).
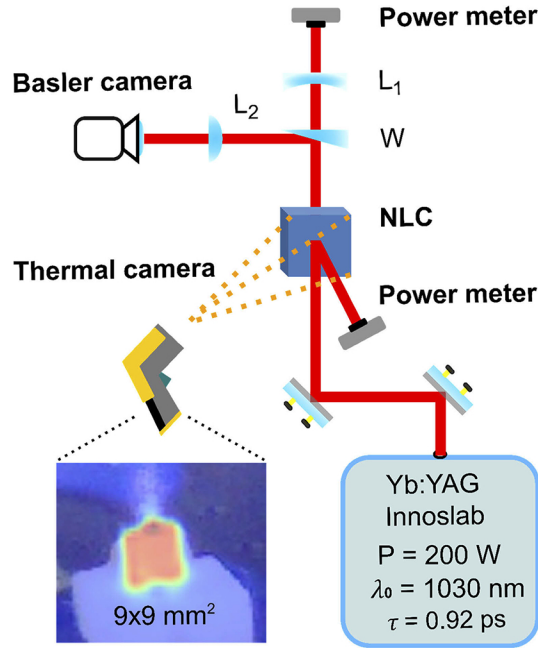
Fig. 1. Thermal imaging setup: All nonlinear crystals (NLC) were of size $9 \times 9 \times 2$ mm^3 and mounted "free standing" (see text). Power meters were used to estimate the power inside the crystal and to confirm the expected Fresnel reflections at both front and back surfaces. The thermal camera was used to measure the temperature across the surfaces of the crystal. An example image from the thermal camera is shown (bottom, left). A Basler camera is used to record beam profiles that are modified by the nonlinear response the NLCs.

3. Results and discussion

3.1. Linear and nonlinear absorption coefficients

The major limiting factors in increasing the average power levels of the OPCPAs are thermal effects due to absorption of pump, signal and idler pulses in the NLCs. In the case of mid-IR OPCPAs (6–16 µm), the relatively small conversion efficiency points to negligible absorption of the idler, and effects of absorption of the signal wavelengths are expected to be similar to that of the pump wavelength. Therefore, under these conditions, we expect the pump pulse to dominate the thermal equilibrium conditions of the crystals [30,33].

Under thermal equilibrium, a thermal model is solved analytically to obtain the linear and nonlinear absorption coefficients. The model was developed using known laser parameters and material parameters with the absorption coefficients α (linear), β (multi-photon) as free parameters. The heat equation is derived by considering energy transfer upon laser impact due to black body radiation and convection under thermal equilibrium [30,34]. For high repetition-rate Yb pump lasers, this is justified because the thermal relaxation time is much longer then the temporal gap between consecutive pulses. Basically, in the thermal model it is assumed that the absorbed laser power P_{abs}, which can be expressed as [35]

$$P_{\text{abs}} = C_1 \alpha I + C_2 \beta I^2, \tag{1}$$

is re-emitted. Thus, total heat H exchanged is given by

$$H = H_{\text{black-body}} + H_{\text{convection}} = \sigma \epsilon A (T_C{}^4 - T_R{}^4) + h A (T_C - T_R) \tag{2}$$

which finally results in

$$\sigma \epsilon A(T_C{}^4 - T_R{}^4) + hA(T_C - T_R) = C_1\alpha I + C_2\beta I^2 \tag{3}$$

The heat radiated due to black-body radiation is determined by the Stefan-Boltzmann constant ($\sigma = 5.669 \times 10^{-8}$ Wm^{-2}K^{-4}) [34], the surface emissivity of the crystals were calibrated against a thermal reference because of the transparency range of the thermal camera is in the transmission window of the mid-IR NLCs. For the case of LGS, $\epsilon_{LGS} = 0.6$ (and for the other crystals, $\epsilon_{AGS} = 0.37$, $\epsilon_{LGSe} = 0.42$, $\epsilon_{LIS} = 0.6$ and $\epsilon_{LISe} = 0.44$) is used, the surface area A of the crystal, the crystal temperature T_C and room temperature T_R. A common value for the heat convection coefficient is $h = 10$ Wm^{-2} K^{-1} according to literature [34].

The coefficients C_1 and C_2 are determined by the laser pulse parameters: repetition rate f, radial beam waists $\omega_x\omega_y$ perpendicular to the propagation direction, the temporal width of the pulses τ and by the crystal length L. Integration of the squared hyperbolic secant (sech) function describing the pulse shape gives

$$C_1 = fL(1.206\omega_x\omega_y\tau) \text{ and } C_2 = fL(0.426\omega_x\omega_y\tau). \tag{4}$$

The variation of the average temperature across the crystal surface with increasing pump laser intensity is shown in Fig. 2, in case of the LGS crystal. The temperature is determined from the center of the crystal aperture in the thermal image. The experiments were performed at 1 MHz and 200 kHz repetition rates. The average power inside the crystal is estimated taking into account the losses due to Fresnel reflections by measuring the reflected power from the surfaces of the crystal. The pulse duration and the spatial beam profiles were very similar at both experimental campaigns. The lower pulse energies at high repetition rate (1 MHz) data show a larger contribution from linear absorption, whereas at 200 kHz, and therefore at higher pulse energies, the nonlinear absorption is dominating (also see Fig. 3). This general trend is observed for all non-oxide NLCs under investigation, except for LGSe. In LGSe crystal, strong multi-photon absorption could already be observed in the low energy per pulse data at 1 MHz. By calculating the total heat as a function of pump laser intensity from the recorded thermal images and by fitting the data according to Eq. (3), rough estimates of the linear and nonlinear absorption coefficients are derived for the different NLCs. The α is derived from the linear fit to 1 MHz data, which is then used in 200 kHz data for nonlinear curve fit to obtain the β. Independent measure of the α improves the fitting accuracy for the estimation of β. As an example, the data evaluation for the LGS crystal is shown in Fig. 3.

The estimated values of the linear and nonlinear absorption coefficients for the various crystals are summarized in Table 1; values for the bandgap and d_{eff} were taken from [36] and [37], respectively. The fitting error for all graphs was less than 0.2%. However, because all systematic errors tend to increase the estimated values using these methods [30], all experimental derived values are given as upper limits (also see discussion in Section 1).

Furthermore, for all non-oxide NLCs, we observed the generation of second harmonic like 'green' light along with increased lensing effects at high intensities; however, too small to affect the analysis of this work. The AGS crystal showed a large Kerr lensing effect already at an average power of 45 W, both in the 1 MHz and 200 kHz data sets, which corresponds to peak intensities of ≈ 0.8 GW/cm^2 and ≈ 4.2 GW/cm^2, respectively. Therefore, the experiments on AGS were not carried out further for higher power levels to avoid damage of the crystal. A similar observation was made in case of LISe as well. In case of the AGS crystal, to within experimental error only a linear increase in temperature was observed for both repetition rates. Thus, only the linear absorption coefficient was obtained for AGS.
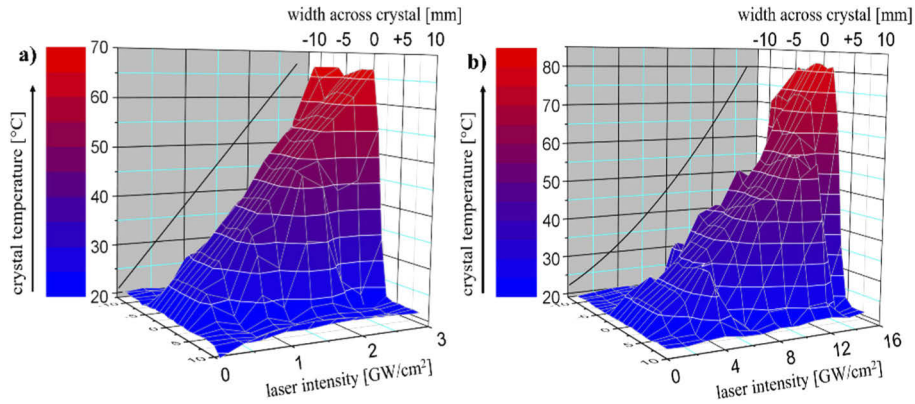
Fig. 2. An example temperature profile using the LGS crystal obtained from thermal images of the crystal recorded by increasing the irradiation power levels inside the crystal at 1 MHz (a) and 200 kHz (b) repetition rates. The average temperature across the crystal as a function of laser intensity is represented by the black line.
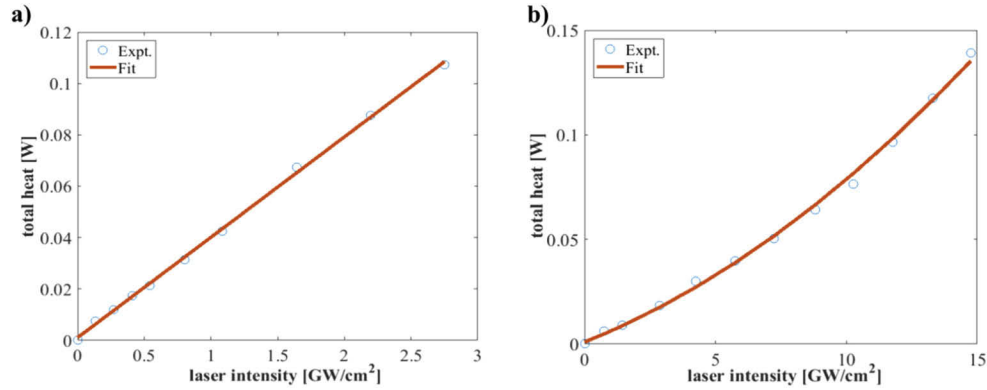

Fig. 3. Linear (a) at 1 MHz and nonlinear curve fit at 200 kHz (b) applied to obtain linear and nonlinear absorption coefficients from the analytical model of total heat vs intensity for the LGS crystal.

3.2. Nonlinear refractive index

We propose a simple and robust method to give an upper estimate of the second-order nonlinear refractive index n_2 of nonlinear crystals based on beam profile measurements after traversing the crystal under realistic high power user conditions and beam parameters. Note that cascaded second-order effects and Kerr lensing can contribute to an effective n_2 [38,39], which is an important parameter for the OPCPA design. In order to benchmark the measurements, we chose uncoated LGS as a sample material, because its effective n_2 value upon high-power pumping at 1 μm has been published recently: 3.5×10^{-15} cm^2/W [23] and 4.1×10^{-15} cm^2/W [29]. The latter study utilized the well-known z-scan method introduced in 1990 by van Stryland and co-workers [32].

The Basler camera images were taken after the beam had passed the "free standing" NLC and imaged into the camera with a wedge (W) and lens ($L_2 = 400$ mm focal length) (see Fig. 1). The results for the LGS crystal are shown in Fig. 4. At 1 MHz, thus relatively low intensity, the beam profiles remain similar (with and without the NLC crystal), and therefore we can also neglect the effects of thermal lensing. But at 200 kHz, the beam profiles show a reduction in the
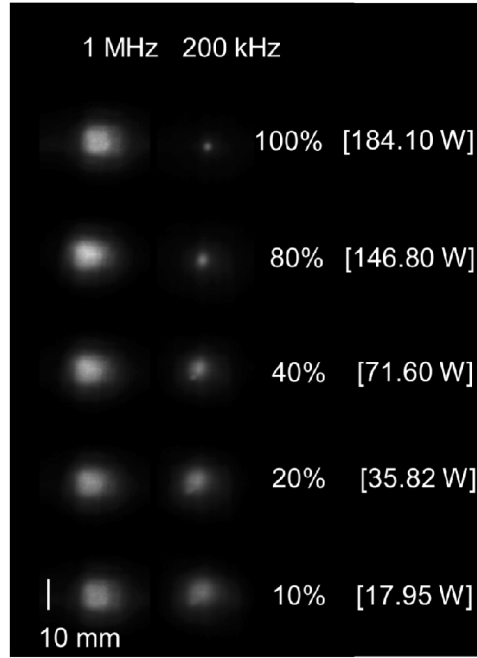
Fig. 4. Basler camera images of the beam profile demonstrating the nonlinear response with increasing pump intensity for the crystal LGS for both 1 MHz and 200 kHz repetition rate. The beam profiles from top to bottom are given for applied laser pump power of 100%, 80%, 40%, 20% and 10% of total power (corresponding estimated crystal internal power is in square brackets).

beam diameter with increasing pump intensity resulting from Kerr lensing (Fig. 4). The beam profile measurements were implemented in order to monitor these processes and to identify, if any irreversible damage occurs during the measurement.

According to the electro-optic (Kerr) effect, a Kerr lens is formed with focal length f_K given by

$$f_K = \omega^2/(4n_2IL). \tag{5}$$

Here, ω is the $1/e^2$ beam radius (determined by the knife-edge method), I describes the peak intensity and L denotes the length of the crystal. Thus with increasing pump intensity, the nonlinear crystal forms an effective lens, reducing the original size of the pump profile, which is measured without a NLC or at very low intensities. Assuming Gaussian beam propagation and known laser, crystal and imaging optics, we derive f_K by comparing the images at various intensities with a simple simulation of Gaussian beam propagation using idealized lenses. In case of LGS crystal, we can provide an upper estimate of $n_2 < 6.4 \times 10^{-15}$ cm^2/W, which is in very good agreement to the published experimental results. The derived second-order nonlinear refractive index n_2 values of all other crystals under investigations are summarized in the Table 1.

4.   Summary and conclusion

Only few suitable nonlinear crystals are available in the mid-IR (6–16 μm), a spectral region of great importance for vibrational molecular spectroscopy and atmospheric sensing. And therefore, in this paper we measure critical material properties of a range of NLCs pumped at 1 μm, which can be used as input for realistic simulations of high-average power laser performance.

Although the well-known AGS crystal has a high d_{eff}, it has a lower bandgap and a much higher nonlinear refractive index (n_2) compared to the other Lithium-based crystals when pumped at 1 μm (Table 1), making this crystal not suitable for high energy and power applications. For low power applications, LIS and LISe might be promising, because they have a relatively high d_{eff}. But for high energy and power applications, LGS crystals combine sufficiently large d_{eff} with a comparatively high optical damage threshold due to the large bandgap and broad transparency range. Additionally, LGS has the lowest multi-photon absorption coefficient and nonlinear refractive index (see Table 1). This makes the material a very promising candidate among the nonlinear non-oxide crystals for high power ultrashort mid-IR OPCPA applications pumped directly at 1 μm.

The presented data provides crucial design parameters for the development of high-average-power mid-IR OPCPA systems based on industrial Yb pump laser technology under realistic user conditions. Finally, we would like to mention that an interesting alternative avenue is of course to use Ho/Tm doped high-power lasers to directly pump suitable nonlinear crystals at 2 μm. However, the challenge is to further boost the pulse energy and average power of these 2-μm pump lasers in order to make full use of the corresponding high effective nonlinearity of the available nonlinear crystals.

Disclosures. The authors declare no conflicts of interest.

References

1. S. Qu, H. Liang, K. Liu, X. Zou, W. Li, Q. J. Wang, and Y. Zhang, "9 μm few-cycle optical parametric chirped-pulse amplifier based on LiGaS$_2$," Opt. Lett. **44**(10), 2422 (2019).
2. M. A. Jakob, M. Namboodiri, M. J. Prandolini, and T. Laarmann, "Generation and characterization of tailored MIR waveforms for steering molecular dynamics," Opt. Express **27**(19), 26979 (2019).
3. T. Südmeyer, E. Innerhofer, F. Brunner, R. Paschotta, T. Usami, H. Ito, S. Kurimura, K. Kitamura, D. C. Hanna, and U. Keller, "High-power femtosecond fiber-feedback optical parametric oscillator based on periodically poled stoichiometric LiTaO$_3$," Opt. Lett. **29**(10), 1111 (2004).
4. F. Mörz, T. Steinle, A. Steinmann, and H. Giessen, "Multi-Watt femtosecond optical parametric master oscillator power amplifier at 43 MHz," Opt. Express **23**(18), 23960 (2015).
5. T. Steinle, F. Mörz, A. Steinmann, and H. Giessen, "Ultra-stable high average power femtosecond laser system tunable from 1.33 to 20 mm," Opt. Lett. **41**(21), 4863 (2016).
6. F. Adler, K. C. Cossel, M. J. Thorpe, I. Hartl, M. E. Fermann, and J. Ye, "Phase-stabilized, 1.5 W frequency comb at 2.8–4.8 mm," Opt. Lett. **34**(9), 1330 (2009).
7. I. Pupeza, D. Sanchez, J. Zhang, N. Lilienfein, M. Seidel, N. Karpowicz, T. Paasch-Colberg, I. Znakovskaya, M. Pescher, W. Schweinberger, V. Pervak, E. Fill, O. Pronin, Z. Wei, F. Krausz, A. Apolonski, and J. Biegert, "High-power sub-two-cycle mid-infrared pulses at 100 MHz repetition rate," Nat. Photonics **9**(11), 721–724 (2015).
8. A. Schliesser, N. Picqué, and T. W. Hänsch, "Mid-infrared frequency combs," Nat. Photonics **6**(7), 440–449 (2012).
9. F. Bach, M. Mero, M.-H. Chou, and V. Petrov, "Laser induced damage studies of LiNbO$_3$ using 1030-nm, ultrashort pulses at 10-1000 kHz," Opt. Mater. Express **7**(1), 240 (2017).
10. F. Bach, M. Mero, V. Pasiskevicius, A. Zukauskas, and V. Petrov, "High repetition rate, femtosecond and picosecond laser induced damage thresholds of Rb:KTiOPO$_4$ at 1.03 μm," Opt. Mater. Express **7**(3), 744 (2017).
11. O. Novák, P. R. Krogen, T. Kroh, T. Mocek, F. X. Kärtner, and K.-H. Hong, "Femtosecond 8.5 μm source based on intrapulse difference-frequency generation of 2.1 μm pulses," Opt. Lett. **43**(6), 1335 (2018).
12. M. Beutler, I. Rimke, E. Büttner, P. Farinello, A. Agnesi, V. Badikov, D. Badikov, and V. Petrov, "Difference-frequency generation of ultrashort pulses in the mid-IR using Yb-fiber pump systems and AgGaSe$_2$," Opt. Express **23**(3), 2730 (2015).
13. M. Knorr, J. Raab, M. Tauer, P. Merkl, D. Peller, E. Wittmann, E. Riedle, C. Lange, and R. Huber, "Phase-locked multi-terahertz electric fields exceeding 13 MV/cm at a 190 kHz repetition rate," Opt. Lett. **42**(21), 4367 (2017).
14. C. Gaida, M. Gebhardt, T. Heuermann, F. Stutzki, C. Jauregui, J. Antonio-Lopez, A. Schülzgen, R. Amezcua-Correa, A. Tünnermann, I. Pupeza, and J. Limpert, "Watt-scale super-octave mid-infrared intrapulse difference frequency generation," Light: Sci. Appl. **7**(1), 94 (2018).
15. J. Zhang, K. F. Mak, N. Nagl, M. Seidel, D. Bauer, D. Sutter, V. Pervak, F. Krausz, and O. Pronin, "Multi- mW, few-cycle mid-infrared continuum spanning from 500 to 2250 cm^{-1}," Light: Sci. Appl. **7**(2), 17180 (2018).

16. G. M. Archipovaite, P. Malevich, E. Cormier, T. Lihao, A. Baltuska, and T. Balciunas, "Efficient few-cycle mid-IR pulse generation in the 5-11 μm window driven by an Yb amplifier," in *Advanced Solid State Lasers* (Optical Society of America, 2017) paper AM4A.4.

17. A. Lanin, A. Voronin, E. Stepanov, A. Fedotov, and A. Zheltikov, "Multioctave, 3–18 μm sub-two-cycle supercontinua from self-compressing, self-focusing soliton transients in a solid," Opt. Lett. **40**(6), 974 (2015).

18. H. Liang, P. Krogen, Z. Wang, H. Park, T. Kroh, K. Zawilski, P. Schunemann, J. Moses, L. F. DiMauro, F. X. Kärtner, and K.-H. Hong, "High-energy mid-infrared sub-cycle pulse synthesis from a parametric amplifier," Nat. Commun. **8**(1), 141 (2017).

19. L. von Grafenstein, M. Bock, D. Ueberschaer, K. Zawilski, P. Schunemann, U. Griebner, and T. Elsaesser, "5 μm few-cycle pulses with multi-gigawatt peak power at a 1 kHz repetition rate," Opt. Lett. **42**(19), 3796 (2017).

20. D. Sanchez, M. Hemmer, M. Baudisch, S. Cousin, K. Zawilski, P. Schunemann, O. Chalus, C. Simon-Boisson, and J. Biegert, "7 μm, ultrafast, sub-millijoule-level mid-infrared optical parametric chirped pulse amplifier pumped at 2 μm," Optica **3**(2), 147 (2016).

21. T. Kanai, P. Malevich, S. S. Kangaparambil, K. Ishida, M. Mizui, K. Yamanouchi, H. Hoogland, R. Holzwarth, A. Pugzlys, and A. Baltuska, "Parametric amplification of 100 fs mid-infrared pulses in ZnGeP$_2$ driven by a Ho:YAG chirped-pulse amplifier," Opt. Lett. **42**(4), 683 (2017).

22. V. Petrov, "Parametric down-conversion devices: The coverage of the mid-infrared spectral range by solid-state laser sources," Opt. Mater. **34**(3), 536–554 (2012).

23. M. Seidel, X. Xiao, S. A. Hussain, G. Arisholm, A. Hartung, K. T. Zawilski, P. G. Schunemann, F. Habel, M. Trubetskov, V. Pervak, O. Pronin, and F. Krausz, "Multi-watt, multi-octave, mid-infrared femtosecond source," Sci. Adv. **4**(4), eaaq1526 (2018).

24. S. B. Penwell, L. Whaley-Mayda, and A. Tokmakoff, "Single-stage MHz mid-IR OPA using LiGaS$_2$ and a fiber laser pump source," Opt. Lett. **43**(6), 1363 (2018).

25. B.-H. Chen, E. Wittmann, Y. Morimoto, P. Baum, and E. Riedle, "Octave-spanning single-cycle middle-infrared generation through optical parametric amplification in LiGaS$_2$," Opt. Express **27**(15), 21306 (2019).

26. B.-H. Chen, T. Nagy, and P. Baum, "Efficient middle-infrared generation in LiGaS$_2$ by simultaneous spectral broadening and difference-frequency generation," Opt. Lett. **43**(8), 1742 (2018).

27. K. Kaneshima, N. Ishii, K. Takeuchi, and J. Itatani, "Generation of carrier-envelope phase-stable mid-infrared pulses via dual-wavelength optical parametric amplification," Opt. Express **24**(8), 8660 (2016).

28. L. Isaenko, A. Yelisseyev, S. Lobanov, A. Titov, V. Petrov, J.-J. Zondy, P. Krinitsin, A. Merkulov, V. Vedenyapin, and J. Smirnova, "Growth and properties of LiGaX$_2$ (X = S, Se, Te) single crystals for nonlinear optical applications in the mid-IR," Cryst. Res. Technol. **38**(35), 379–387 (2003).

29. M. Mero, L. Wang, W. Chen, N. Ye, G. Zhang, V. Petrov, and Z. Heiner, "Laser-induced damage of nonlinear crystals in ultrafast, high-repetition-rate, mid-infrared optical parametric amplifiers pumped at 1 μm," Proc. SPIE **11063**, 1106307 (2019).

30. R. Riedel, J. Rothhardt, K. Beil, B. Gronloh, A. Klenke, H. Höppner, M. Schulz, U. Teubner, C. Kränkel, J. Limpert, A. Tünnermann, M. J. Prandolini, and F. Tavella, "Thermal properties of borate crystals for high power optical parametric chirped-pulse amplification," Opt. Express **22**(15), 17607 (2014).

31. A. Alexandrovski, M. Fejer, A. Markosyan, and R. Route, "Photothermal common-path interferometry (PCI): new developments," Proc. SPIE **7193**, 71930D (2009).

32. M. Sheik-Bahae, A. A. Said, T.-H. Wei, D. J. Hagan, and E. W. van Stryland, "Sensitive measurement of optical nonlinearities using a single beam," IEEE J. Quantum Electron. **26**(4), 760–769 (1990).

33. M. K. R. Windeler, K. Mecseki, A. Miahnahri, J. S. Robinson, J. M. Fraser, A. R. Fry, and F. Tavella, "100 W high-repetition-rate near-infrared optical parametric chirped pulse amplifier," Opt. Lett. **44**(17), 4287 (2019).

34. M. Sabaeian, F. S. Jalil-Abadi, M. M. Rezaee, A. Motazedian, and M. Shahzadeh, "Temperature distribution in a Gaussian end-pumped nonlinear KTP crystal: the temperature dependence of thermal conductivity and radiation boundary condition," Braz. J. Phys. **45**(1), 1–9 (2015).

35. S. Seidel and G. Mann, "Numerical modeling of thermal effects in nonlinear crystals for high average power second harmonic generation," Proc. SPIE **2989**, 204 (1997).

36. L. I. Isaenko and A. P. Yelisseyev, "Recent studies of nonlinear chalcogenide crystals for the mid-IR," Semicond. Sci. Technol. **31**(12), 123001 (2016).

37. A. V. Smith, "SNLO nonlinear optics code (free version)" from http://www.as-photonics.com/snlo.

38. R. DeSalvo, D. J. Hagan, M. Sheik-Bahae, G. Stegeman, and E. W. Van Stryland, "Self-focusing and self-defocusing by cascaded second-order effects in KTP," Opt. Lett. **17**(1), 28 (1992).

39. M. Falconieri, "Thermo-optical effects in z-scan measurements using high-repetition-rate lasers," J. Opt. A: Pure Appl. Opt. **1**(6), 662–667 (1999).